Combined Maximum Power Point and Yaw Control Strategy for a Horizontal Axis Wind Turbine

A. Mesemanolis and C. Mademlis

***Abstract* -- In this paper, a combined maximum power point tracking (MPPT) and active yaw control strategy for a wind energy conversion system (WECS) is presented. The proposed control system provides maximum power point operation of the wind turbine combined with fast and reliable alignment of the nacelle to the wind direction and therefore, maximization of the captured power from the incident wind. For the implementation of the MPPT control, the rotor speed is required, while for the implementation of the yaw control, only the measurement of the wind speed is needed because the wind direction, and therefore the yaw angle, can be estimated from the error between the optimum and the real mechanical power at the shaft. The drive train of the WECS comprises a three blade horizontal axis wind turbine coupled to a three-phase squirrel cage induction generator (SCIG) driven by two back-to-back converters operating with space vector modulation. The active yawing is implemented by utilizing a position controlled squirrel cage induction motor (SCIM) drive. Simulation results are presented for the validation of the theoretical considerations and the demonstration of the effectiveness of the proposed control scheme.**

***Index Terms*—Yaw control, squirrel cage induction generator, wind power generation, wind energy, optimal control, variable speed motor drives.**

NOMENCLATURE

I_{ds}, I_{qs}	*d*- and *q*-axis components of the induction generator stator current, respectively,
I_{dN}, I_{qN}	*d*- and *q*-axis components of the grid current, respectively,
L_m , L_r	magnetizing and rotor inductance of the induction generator, respectively,
P_w	wind power,
P_{wt}	mechanical power produced by the wind turbine, at the case that it is aligned to wind direction,
P_{wt_γ}	mechanical power produced by the wind turbine under misalignment between the nacelle and wind direction (yawed power),
P_e	electrical output power of the generator,
Q_N	reactive power injected to the grid,
C_p	wind turbine power coefficient,
u	wind speed in m/s,
n	gear ratio of the gear box,
λ	tip speed ratio of the wind turbine,
ω_e	stator frequency in rad/s,
ω_{wt}	angular velocity of the wind turbine shaft,
ω_r	angular velocity of the electric generator shaft ($\omega_r = n\,\omega_{wt}$),
p	induction generator pole pairs,
T_{wt}	torque produced by the wind turbine,
T_{rm}	torque on the generator shaft ($T_{rm} = T_{wt}/n$),
T_{ml}	torque loss at the speed-up side of the gear box,
T_e	induction generator electromagnetic torque,
γ	yaw-angle (misalignment between the nacelle and the wind direction).

This work was supported by European Regional Development Funds and Greek National Resources (Ministry of Education, Lifelong Learning Fund and Religious Affairs, Greece under Research Grant 09SYN-32-624, Research Program "Cooperation 2009").

A. Mesemanolis and C. Mademlis are with the Department of Electrical Energy, School of Electrical and Computer Engineering, Faculty of Engineering, Aristotle University of Thessaloniki, GR-54124, Thessaloniki, Greece (e-mail: mademlis@eng.auth.gr).

INTRODUCTION

DURING the last decades, wind energy conversion systems have attracted increased attention as an infinite source of power, capable of sustaining the ever growing worldwide power needs. The development on aerodynamics and power electronics have allowed construction of more efficient wind energy conversion systems, capable of producing hundreds of megawatts of electrical power.

In order to take full advantage of the incident wind power, the MPPT and the yawing problems need to be solved. Extensive work can be found on the literature regarding the MPPT control and a number of algorithms have been proposed for the adjustment of the rotational speed of the wind turbine. Most notable MPPT methods are that based on the optimal tip speed ratio [1]-[3], perturbation and observation (P&O) method [4]-[6], fuzzy-logic control [7]-[11], artificial neural networks [12] and torque controlled MPPT [13]-[16].

Contrary to the high research interest on MPPT techniques, the problem of aligning the wind turbine with the wind direction has not been extensively addressed in the literature. Significant research work has been conducted on the aerodynamics of wind turbines and specifically, the aerodynamic phenomena that follow the operation of a wind turbine have been extensively investigated [17]-[27]. Thus, considerable knowledge has been produced that aids the development of a suitable yaw control system for optimum operation of wind turbines.

It is well known that measurement of the wind direction through a direct measuring unit at the rear end of a wind turbine is inaccurate due to the wake effect of the wind turbine blades. Specifically, wind interaction with the turbine blades causes turbulence behind the blade which results in heavy distortion of the measurement. Contrarily, it is possible to obtain a satisfactorily accurate measurement of the wind speed, by applying appropriate calibration at the wind sensor and averaging of the measurements over several turbine rotations. Due to the fast dynamics of the wind speed magnitude, the above method is not appropriate for use with an MPPT technique, because the wind speed may change during the averaging period, resulting to

978-1-4799-4389-0/14/$31.00 ©2014 IEEE

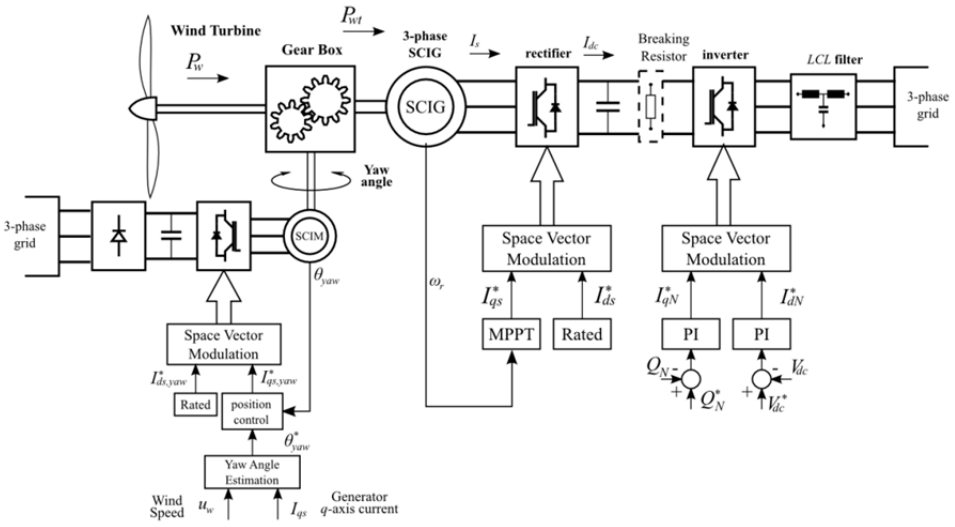

Fig. 1. Structure of the WECS drive train and the yaw system.

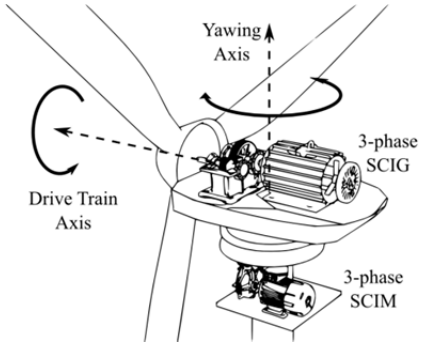

Fig. 2. Schematic representation of the active yawing mechanism.

misleading measurements. However, this measurement can be suitable for the estimation of the wind direction because the wind direction does not change as fast as the wind speed.

From the above it is concluded that yaw control of WECSs remains an open issue, due to uncertainties caused by the measurement of the wind. Aim of this paper is to propose a combined control method that achieves both maximum power point operation and successful alignment of the wind turbine with the direction of the incident wind through an active yawing mechanism. The proposed control scheme achieves increased wind power extraction from the incident wind which results to increased electrical power production. The suggested yaw control is accomplished without the knowledge of the wind direction, since the yaw angle is estimated from the error between the optimum and the real mechanical power at the shaft. Thus, the yaw control is more reliable and also the overall cost of the WECS is reduced because the wind direction sensor is not required.

The proposed system comprises a wind turbine coupled to a SCIG through a gearbox. The generator is connected to the grid through two back-to-back converters, operating with space vector modulation. Thus, full control over the generator and injection of the produced power to the electrical grid with minimum harmonic distortion is achieved, as required by the grid manager. Rotor field oriented control is employed for the SCIG with the *q*-axis current component of the generator regulating the torque, while the *d*-axis current component adjusts the flux-linkage of the machine. For the MPPT control strategy, torque control is employed and specifically, the *q*-axis current of the generator is adjusted according to the control law established by the MPPT condition of the wind turbine. Thus, the MPPT control is implemented without the measurement of the wind speed.

The yawing mechanism is actuated by a three-phase SCIM driven by a power converter and operating with position control. The direction of the wind turbine is adjusted at regular intervals such that the wind turbine to be aligned with the wind direction. The yaw angle of the incident wind is estimated at regular intervals using information from the wind speed measurement sensor and the MPPT algorithm, so as the alignment of the nacelle with the wind direction is accordingly accomplished.

Several simulation results are presented in order to validate the effectiveness and operational improvements of the proposed control scheme.

WECS CONFIGURATION

Fig.1 illustrates the block diagram of the optimally controlled WECS. The wind turbine is coupled to the shaft of a SCIG through a gear box that is inserted in order to adapt the low rotational speed of the wind turbine to the high speed of the generator. The SCIG is connected to the power grid through two back-to-back converters, both utilizing the space vector control technique. The *LCL* filter between the inverter and the grid reduces the harmonic currents injected to the grid. A dynamic braking resistor is established in the *dc*-link, in order to dissipate the excess electrical energy that cannot be absorbed by the grid.

The active yawing system is installed at the connection of the nacelle to its supporting column (Fig. 2). The system comprises a three-phase SCIM which is driven through an appropriate power converter. The SCIM is mechanically coupled to the pylon bearings through a bevel gearbox reducer which increases the torque and decreases the speed of the generator in order to achieve higher precision of the

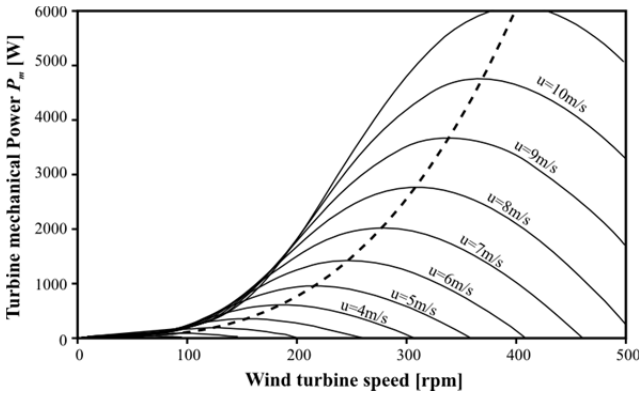

(a)

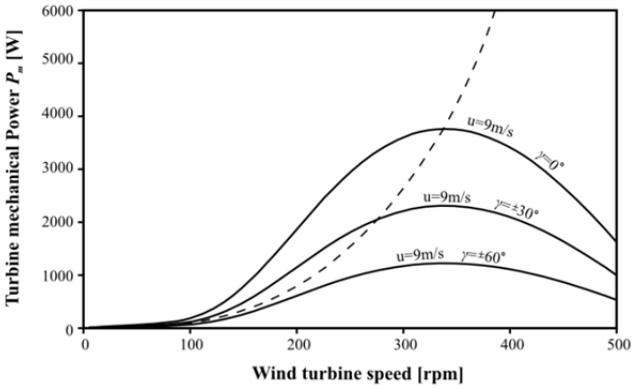

(b)

Fig. 3. Mechanical power output of the wind turbine: (a) for various wind and rotor speed values for the case that the turbine is aligned to wind direction (yaw angle is equal to zero, $\gamma = 0^0$) and (b) for constant wind speed 9m/s and various yaw angles γ. For both diagrams, the MPP locus is represented by the dashed curve.

position control. Due to mechanical restrictions, the rotational speed of the nacelle needs to be very low and therefore a reducer with high gear ratio is used.

The control system for the WECS drive train employs rotor field oriented control with space vector modulation, thus independent regulation of the *q*- and *d*- axis current components is possible. The *d*- axis current component is used to provide rated flux linkage to the generator. The *q*-axis current component is directly proportional to the torque of the generator and therefore it is controlled in order to regulate the rotational speed of the generator according to an MPPT condition.

For the line-side inverter, the vector control method with space vector modulation is employed as well. The *d*-axis current component of the inverter is controlled through a PI controller in order to keep constant the *dc*-link voltage and thus, to control the active power. The *q*-axis current component of the inverter is controlled through another PI controller in order to regulate the line-side power factor and thus, to provide the demanded reactive power to the grid.

The yawing control system comprises two control loops. The inner control loop regulates the rotational speed of the yaw motor through a PI that adjusts the *q*-axis current component of the yaw motor drive, while the outer control loop controls the position of the yaw motor.

WIND TURBINE CHARACTERISTICS

The power captured by a wind turbine is given by

$$P_{wt} = \frac{1}{2}\rho A C_p u^3 \tag{1}$$

where ρ is the air density (typically 1.25 kg/m^3), A is the swept area (cross-sectional area) of the turbine (in m^2), C_p is the wind-turbine power coefficient and u is the wind speed (in m/s). The coefficient C_p depends on the pitch angle of the blades β (in degrees) and the tip-speed ratio λ, which is defined as the ratio of the linear velocity of the blade tip ($\omega_{wt}R$) to the wind speed u as follows

$$\lambda = \frac{\omega_{wt}R}{u} \tag{2}$$

where ω_{wt} is the wind turbine shaft speed (in rad/s) and R is the radius of the blades (in m). For each blade pitch angle β, the value of the tip-speed ratio is constant for all MPPs and from it is concluded that the optimum rotor speed $\omega_{wt_{opt}}$ at a wind speed u is calculated by

$$\omega_{wt_{opt}} = \frac{\lambda_{opt}u}{R} \tag{3}$$

The relation of C_p versus λ is obtained by the following equation that is commonly used in wind turbine simulators [12]

$$C_p(\lambda,\beta) = 0.5176\left(\frac{116}{\lambda_i} - 0.4\beta - 5\right)e^{-\frac{5}{\lambda_i}} + 0.0068\lambda \tag{4}$$

with

$$\frac{1}{\lambda_i} = \frac{1}{\lambda + 0.08\beta} - \frac{0.035}{\beta^3 + 1} \tag{5}$$

A three-blade horizontal axis wind turbine with radius of 2.25 m is used at the system. Fig. 3 illustrates the steady state power-speed characteristics (solid curves) and the maximum power point curve (dashed curve) attained at each wind speed, for a blade pitch angle of 0 degrees ($\beta = 0^0$).

The torque produced by the wind turbine can be calculated from

$$T_{wt} = P_{wt}/\omega_{wt} = C_T(\lambda,\beta)\frac{\rho\pi R^3}{2}u^2 \tag{6}$$

where $C_T(\lambda,\beta) = C_P(\lambda,\beta)/\lambda$ is the wind turbine torque coefficient. Since a gear box is used, the wind turbine speed and torque is converted to the machine level on the basis of the gear ratio n as follows: $\omega_r = n\,\omega_{wt}$ and $T_{rm} = T_{wt}/n$ where ω_r and T_{rm} are the mechanical speed and torque of the generator, respectively.

When the wind meets the turbine blades under a yawed angle, the effective wind speed decreases, because the effective area of the rotor is reduced. Under a yaw angle, the aerodynamic coefficient C_p is reduced by the cube of

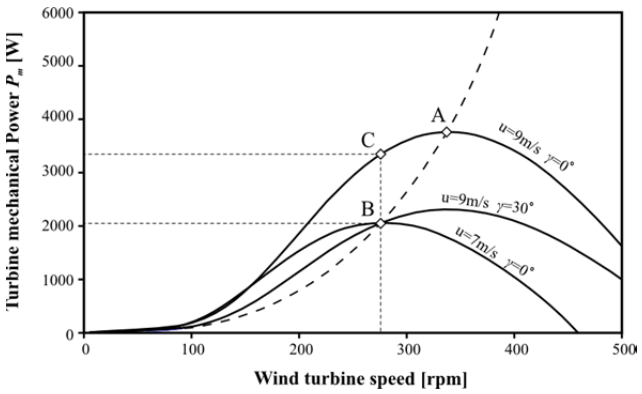

Fig. 4. Yawing effect at the wind turbine, for wind speed 9 m/s. As yaw angle increases, the wind curves are shrunken and the operating point deviates from the MPP. At the new operating point B, the turbine mechanical power is reduced due to yaw error and the loss of MPPT control. Thus, although the wind speed is 9m/s, the behavior of the turbine is similar to 7m/s.

the cosine of the yaw angle γ, as follows

$$C_p(\lambda,\beta,\gamma) = C_p(\lambda,\beta)\cos^3\gamma \tag{7}$$

and consequently, the wind turbine power is accordingly reduced [27].

MPPT Strategy

From the previous analysis, it is understood that at a certain tip speed ratio λ, maximum power harvesting from the incident wind can be achieved. Thus, the maximum produced torque at the turbine shaft is obtained for optimum $C_{p_{opt}}$ coefficient and optimum tip speed ratio λ_{opt} and rotor speed $\omega_{r_{opt}}$, and is given by

$$T_{rm_{opt}} = \frac{\rho\pi R^5}{2n^3\lambda_{opt}^3} C_{p_{opt}} \omega_{r_{opt}}^2 \tag{8}$$

Due to mechanical loss that the bearings and the intermediate gear box may cause, the electromagnetic torque at the generator is given by

$$T_{e_{opt}} = T_{rm_{opt}} - T_{ml} \tag{9}$$

where T_{ml} is the mechanical loss torque. The mechanical losses torque is proportional to the square of the rotating speed and therefore (9) becomes

$$T_{e_{opt}} = \left[\frac{\rho\pi R^5}{2n^3\lambda_{opt}^3} C_{p_{opt}} - c_m\right]\omega_{r_{opt}}^2 \tag{10}$$

In field-oriented control on SCIG, decoupled control of *d*- and *q*-axis stator current components is provided by aligning the rotor flux linkage ψ_r to the *d*-axis ($\psi_{dr} = \psi_r$ while $\psi_{qr} = 0$). Due to decoupled control of the *d*- and *q*-axis stator currents, the electromagnetic torque expression is given by [28]

$$T_e = \frac{3}{2} p \frac{L_m^2}{L_r} I_{qs} I_{ds} \tag{11}$$

Since the *d*-axis current component is maintained at the rated value in order to achieve rated flux-linkage at the generator, the electromagnetic torque at the generator shaft is directly proportional to the *q*-axis current component. From (10) and (11), the optimum *q*-axis current component that provides MPPT is given by

$$I_{qs_{opt}} = L_r \frac{\rho\pi R^5 C_{p_{opt}} - 2c_m n^3 \lambda_{opt}^3}{3pL_m^2 n^3 \lambda_{opt}^3 I_{ds}} \omega_r^2 = c\omega_r^2 \tag{12}$$

The constant *c* of (12) can be initially estimated using the generator and turbine parameters and then it can be fine-tuned through a training algorithm in order to compensate for modeling and parameters inaccuracies.

Following the condition (12) for the *q*-axis current component regulation, the wind turbine always finds a stable equilibrium at the optimal rotational speed and therefore, it always follows the MPP of the wind turbine. Thus, maximum power is always harvested, as long as the turbine is aligned with the direction of the incident wind. Note that, since for the MPPT algorithm the measurement of the wind is not required, the MPPT is fast and reliable.

The operation of the MPPT can be qualitatively explained in Fig. 3a. The dashed line represents the locus of the MPPs of the turbine for any wind speed. Specifically, when the rotational speed of the generator is lower than the optimum, the induced torque of the turbine is higher and tends to accelerate the rotor towards the MPP. Contrarily, when the rotational speed is above the optimal, the generator torque is higher and decelerates the rotor. Therefore, the above MPPT control provides stable operation at any wind speed.

Yaw Control Strategy

Form (7) it is concluded that, if a misalignment of an angle γ occurs between the nacelle and wind direction, the coefficient C_p is reduced and consequently the curves of the turbine are shrunken. In that case, due to the MPPT control, the equilibrium will be shifted towards a rotational speed ω_r lower than the optimal. As can be seen in Fig. 3b, if the yaw angle is increased, the wind turbine mechanical power is decreased and consequently, the electric power that the WECS can produce is reduced. Therefore, the yaw control should operate alongside the MPPT and track the direction of the wind by adjusting the direction of the nacelle at regular intervals.

The yawing effect at the wind turbine, for constant wind speed 9m/s, is explained in Fig. 4. The quadratic relationship between the torque of the generator and the rotational speed of the turbine ensures that the turbine operates at the MPP, according to the procedure described in Section IV. Thus, at a wind speed of 9m/s, the torque will be accordingly adjusted so as the equilibrium will be at point A. However, when there is a misalignment between the wind and the turbine, the C_p curves are shrunken as per (7). Following the quadratic relation of MPPT controller, the power output will be reduced and the equilibrium will be shifted away from the MPP, at point B. By operating at point B and although the wind speed is 9 m/s, the MPPT control is misguided and the turbine operates as if the wind

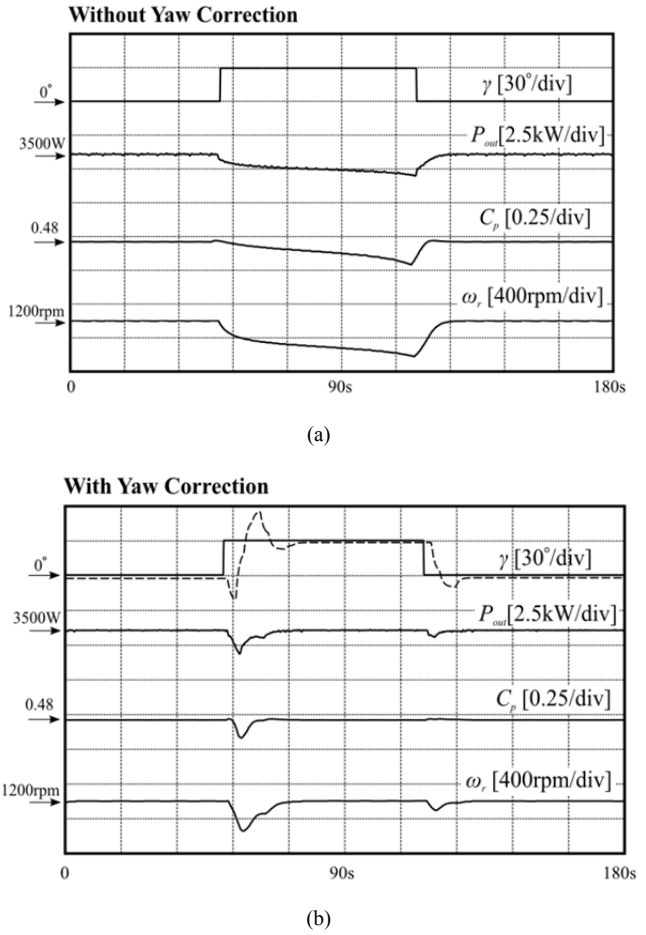

Fig. 5. Simulation results of the WECS operation with constant wind speed of 9m/s and a step change in the wind direction of 30 degrees: (a) operation without yaw correction and (b) operation with yaw correction (the dashed line represents the yaw angle of the wind turbine).

speed was 7 m/s. This would result to further reduction of the wind turbine power. From the above it is concluded that, the turbine power reduction due to misalignment of the turbine to wind direction is not only owed to aerodynamic reasons, but also to loss of the MPPT control.

The yawed turbine power (point B of Fig. 4) can be calculated from the electromagnetic power plus the mechanical loss, thus

$$P_{wt_\gamma} = \frac{3}{2} p \frac{L_m^2}{L_r} I_{qs} I_{ds} \omega_{wt} + c_m \omega_{wt}^3 \tag{13}$$

The aligned turbine power (point C of Fig. 4) can be calculated from (1) by using the wind turbine curves and the measurements of the wind speed. Since the yawed C_p coefficient is reduced by the cube of the cosine yaw angle (7), the relation of the yawed P_{wt_γ} and the aligned mechanical power of the wind turbine is

$$P_{wt_\gamma} = P_{wt} \cos^3 \gamma \tag{14}$$

and therefore, the yaw angle of the turbine is given by

$$\gamma = \sqrt[3]{\frac{P_{wt_\gamma}}{P_{wt}}} \tag{15}$$

From (15) the yaw angle can be estimated; however, due to symmetry, the sign of yaw error cannot be determined. Therefore, the yaw control can be accomplished by following an experimental procedure as described below:

a) During a large time frame, the measurements are acquired and averaged and the yaw angle is calculated from (15). The sign of the yaw error is randomly decided and the nacelle rotates a few degrees towards this direction.
b) During a smaller time frame, the new angle is estimated using (15) and it is compared to that of the previous step. A smaller new yaw error means that the initial assumption for the yaw direction was correct, whereas a larger new yaw error means that the yaw direction was wrong and the nacelle should rotate on the opposite direction.
c) The nacelle rotates to the correct direction (as decided from step-b) and rotates to the final yaw angle (as decided from step-a).

It should be noted that, in order to acquire sufficiently accurate results, the measurements of the wind and power of the turbine should be appropriately averaged over a relatively large time frame. For the purposes of yaw regulation, the time frame should be adequately large and comprise several full rotor rotations. This is because it is related to mechanical time constants for large mechanical bodies such as the system of the nacelle and the rotating blades. A rational time frame for yaw correction would be from 1 to10 minutes, depending on the size and the rated speed of the wind turbine. However, choosing a time frame that is too large may cause extended misalignment of the nacelle and loss of potential energy.

The yaw control of the wind turbine could be examined separately from the MPPT control; however, the present implementation relies on signals acquired from the specific MPPT control strategy. Therefore, the yaw control and the MPPT control are considered coupled, since failure of the one could result to destabilization of the other control algorithm.

Simulation Results

The proposed control scheme has been implemented using the simulation software Matlab/Simulink. A wind turbine with a blade radius of 2.5m has been simulated along with a gear box with a gear ratio of 4. For the drive train, a 3-phase, 50 Hz, 400 V, 5.5-kW squirrel cage induction generator has been considered with a gearbox of 1:5 gear ratio. For the yaw control, a three phase induction motor of 200 W, 50 Hz, 400 V has been used along with a 1:72 gear ratio slew-ring, such us the cost of the installation remains low enough to justify the use of the yaw control system.

The generator is driven by a power converter operating with field oriented control. The *d*-axis current component is maintained at the rated no-load current of 6.5A and the *q*-axis current component is decided by the MPPT condition of (12). At the dc-link, a capacitor of 2mF is used and a breaking resistor of 50 Ω is considered, in order to dissipate the excess electrical energy that cannot be absorbed by the grid, due to overcharge of the generator or grid side faults.

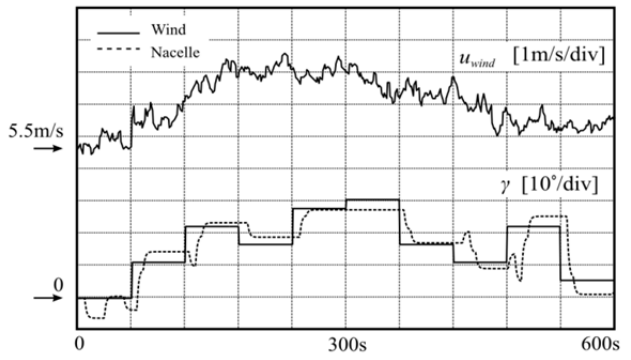

(a)

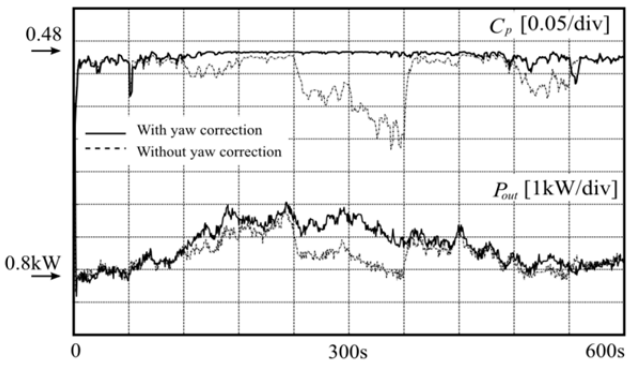

(b)

Fig. 6. Simulation results of the WECS operation with a wind speed and direction profile obtained by measurements. For the Fig. 6a, the solid curves correspond to wind data (speed and direction) and the dotted curve to the nacelle direction. For the Fig. 6b, the solid curves correspond to WECS operation with yaw correction and the dotted curves to WECS operation without yaw correction.

The grid side power converter utilizes voltage oriented control, such as the *d*-axis and *q*-axis current component regulates the active and reactive power respectively. The power flow is regulated through a PI-controller that maintains the voltage of the dc-link at 600V by regulating the *d*-axis current of the inverter. For the simulations, a power factor of unity is considered at the point of common coupling with the grid; however, it can be capacitive or inductive, depending on the grid manager demands. The inverter is connected to the grid through an LCL filter of 4.2mH and 5μF induction and capacitance respectively, in order to reduce current and voltage harmonics at the point of common coupling.

Fig. 5 illustrates the WECS operation under constant wind speed of 9m/s and a step change in the wind direction of 30 degrees. In Fig. 5a, the system operates with MPPT control and the yaw control system is inactive. Initially, the nacelle is aligned with the wind direction and the WECS operates with MPPT control producing electric power of 3.5kW. The maximum value of C_p coefficient is 0.48 that corresponds to MPP operation. Then, a step change of the wind direction is introduced and the electric power production is lowered both due to misalignment of the nacelle and loss of MPP operation. Specifically, loss of MPP operation can be observed through the lowering of the C_p coefficient and the reduction of the rotational speed.

In Fig. 5b, combined operation of the MPPT and yaw control is demonstrated. The same wind speed and wind direction conditions are considered, as in Fig. 5a. The dashed line represents the yaw angle of the wind turbine. When the wind direction changes, the system starts tracking it by initially guessing a false direction and then immediately switching to the correct yaw direction. After four yaw-control steps, the nacelle has been aligned with the wind direction. This is apparent because the coefficient C_p obtains the maximum value of 0.48 and also the WECS produces 3.5kW that corresponds to MPP operation. After the wind angle returns to its initial value (initial wind direction, $\gamma = 0^0$), the system again finds the correct yaw angle and aligns the turbine to the wind direction. It can be seen that, the coefficient C_p returns to its maximum value and the also the WECS produces maximum power.

Fig. 6 illustrates the WECS operation with a wind speed and direction profile obtained by measurements. The wind profile spans from 5.5m/s up to 8.5m/s. The yaw angle changes in steps and it extends from 0 to 30 degrees. The angle of the nacelle direction is illustrated with the dotted curve. It can be seen at the second diagram of Fig. 6a that, the nacelle successfully tracks the wind direction and can follow it even in abrupt and large yaw angle changes.

Fig. 6b illustrates the C_p power coefficient and the turbine power during the above wind speed and direction variation. The respective results are plotted for combined MPPT and yaw control operation (solid curve) along with the results for operation without yaw control (only MPPT control is active, dotted curves). It can be seen that, with both MPPT and yaw control (solid curves), the power coefficient C_p remains close to the value of 0.48, which is the optimum value for the selected type of wind turbine achieving maximum power extraction from the incident wind. Contrarily, if yaw control is inactive (dotted curves) and the nacelle direction deviates from the wind direction, it can be seen that the C_p coefficient and the produced power are reduced compared to their optimal values of solid curves.

From the above simulation results it can be concluded that, for low yaw angles up to 10 degrees, the operation of the wind turbine is not considerably affected. This is due to the fact that the reduction of power follows the cube of the cosine of the yaw angle and therefore, the power reduction is negligible for small yaw angles. However, at larger yaw angles, the power loss at the turbine grows disproportionally and specifically, the power loss results both from the reduction of the wind curves and the loss of MPP.

From Fig. 6a, it can be seen that the yaw control algorithm might produce small error between the nacelle alignment and the wind angle. However, as explained above, at such small yaw angles the difference between the produced power and the optimum is negligible and therefore the yaw algorithm is unable to track it. Practically, the algorithm reaches a steady state with a yaw error smaller than 5 degrees. This effect also prevents from the "over-tracking" of the wind direction and therefore, continuous rotation of the yawing system is avoided that may cause degradation and fatigue of the mechanical parts.

CONCLUSIONS

In this paper, a combined MPPT and yaw control

strategy has been proposed for a horizontal axis WECS. The proposed control system achieves both MPP operation of the wind turbine and alignment of the nacelle with the wind direction. Therefore, maximum power absorption of the incident wind is achieved. The proposed yaw control algorithm estimates the angle misalignment between the nacelle and the wind direction using the measurement of the incident speed and the error between the optimum and the real mechanical power at the shaft. Since a wind direction sensor is not needed, the overall cost of the WECS is reduced and the control of the system is more reliable. An experimental procedure for adjusting the nacelle yaw angle towards the wind directions is reported in the paper. The WECS that is used for the simulations utilizes a SCIG for the rotor drive train and a SCIM for the yawing mechanism. However, the analysis is valid and for any type of electrical machines. Simulation results have been presented for the validation of the theoretical considerations and demonstration of the effectiveness of the proposed scheme.

REFERENCES

[1] E. Hau, '*Wind Turbines, Fundamentals, Technologies, Application, Economics*', Berlin: Springer-Verlag, 2006.

[2] A. Mirecki, X. Roboam, and F. Richardeau, 'Architecture complexity and energy efficiency of small wind turbines', *IEEE Trans. Ind. Electron.*, vol. 54, no. 1, pp. 660-670, Feb. 2007.

[3] R. Datta and V. T. Ranganathan, 'A method of tracking the peak power points for a variable speed wind energy conversion system', *IEEE Trans. Energy Convers.,* vol. 18, no. 1, pp. 163-168, March 2003.

[4] R.M. Hilloowala and A.M. Sharaf, 'A rule-based fuzzy logic controller for a PWM inverter in a stand-alone wind energy conversion scheme', *IEEE Trans. Ind. Appl.*, vol. 32, no. 1, pp. 57-65, Jan./Feb. 1996.

[5] M. Pucci and M. Cirrincione, 'Neural MPPT control of generators with induction machines without speed sensors', *IEEE Trans. Ind. Electron.*, vol. 58, no. 1, pp. 37-47, Jan. 2011.

[6] V. Agarwal, R. K. Aggarwal, P. Patidar, and C. Patki, 'A novel scheme for rapid tracking of maximum power point in wind energy generation systems', *IEEE Trans. Energy Convers.*, vol. 25, no. 1, pp. 228-236, March 2010.

[7] V. Galdi, A. Piccolo, and P. Siano, 'Designing an adaptive fuzzy controller for maximum wind energy extraction', *IEEE Trans. Energy Convers.,* vol. 23, no. 2, pp. 559-569, June 2008.

[8] C.T. Pan and Y.L. Juan, 'A novel sensorless MPPT controller for a high-efficiency microscale wind power generation system', *IEEE Trans. Energy Convers.*, vol. 25, no. 1, pp. 207-216, March 2010.

[9] M. G. Simões, B. K. Bose, and R. J. Spiegel, 'Design and performance evaluation of a fuzzy-logic-based variable-speed wind generation system', *IEEE Trans. Ind. Appl*., vol. 33, no. 4, pp. 956-965, July/Aug. 1997.

[10] A. Mesemanolis, C. Mademlis, and I. Kioskeridis, 'Maximum efficiency of a wind energy conversion system with a PM synchronous generator', in *Proc. MedPower 2010 Int. Conf*., pp. 1-9.

[11] A. Mesemanolis, C. Mademlis, and I. Kioskeridis, 'Maximum Electrical Energy Production of a Variable Speed Wind Energy Conversion System, in *Proc. IEEE ISIE'2012,* pp. 1029-1034.

[12] A. Mesemanolis, C. Mademlis, and I. Kioskeridis, 'High-efficiency control for a wind energy conversion system with induction generator', *IEEE Trans. Energy Convers.,* vol. 27, no. 4, pp. 958-967, Dec. 2012.

[13] A. Mesemanolis, C. Mademlis, and I. Kioskeridis, 'A fuzzy-logic based control strategy for maximum efficiency of a wind energy conversion system', in *Proc. Speedam 2012 Int. Conf.,* pp. 7-12.

[14] A. G. Abo-Khalil, H. G. Kim, D. C. Lee, and J. K. Seok, 'Maximum output power control of wind generation system considering los minimization machines', in *Proc. IEEE Int. Conf. IECON 2004*, pp. 1676-1681.

[15] A. G. Abo-Khalil, 'Model-based optimal efficiency control of induction generator for wind power systems', in *Proc. Conf. Rec. ICIT-2011,* pp. 191-197.

[16] S. Morimoto, H. Nakayama, M. Sanada, and Y. Takeda, 'Sensorless output maximization control for variable-speed wind generation system using IPMSG', *IEEE Trans. Ind. Appl*., vol. 41, no. 1, pp. 60-67, Jan./Feb. 2005.

[17] M.O.L. Hansen, '*Aerodynamics of Wind Turbines*', Earthsgan, 2008.

[18] L.J. Vermeer, J.N. Sorensenb, A. Crespoc, 'Wind turbine wake aerodynamics', *Progress in Aerospace Sciences*, vol. 3, pp. 467–510, 2003

[19] M.S. Adaramola, P.-Å. Krogstad, 'Experimental investigation of wake effects on wind turbine performance', *Renewable Energy,* vol. 36, pp. 2078-2086, 2011.

[20] P. R. Ebert, D. H. Wood, 'The near wake of a model horizontal-axis wind turbine – I. Experimental arrangements and initial results', *Renewable Energy*, vol. 12, No. 3, pp. 225-243, 1997.

[21] P. R. Ebert, D. H. Wood, 'The near wake of a model horizontal-axis wind turbine – II. General features of the three-dimensional flowfield', *Renewable Energy*, vol. 18, pp. 513-534, 1999.

[22] P. R. Ebert, D. H. Wood, 'The near wake of a model horizontal-axis wind turbine – III. Properties of the tip and hub vortices', *Renewable Energy*, vol. 22, pp. 461–472, 2001.

[23] Jang-Oh Mo, Amanullah Choudhr, Maziar Arjomandi, Richard Kelso, Young-Ho Lee, 'Effects of wind speed changes on wake instability of a wind turbine in a virtual wind tunnel using large eddy simulation', *Journal of Wind Engineering and Industrial Aerodynamics*, vol. 117, pp. 38–56, 2013.

[24] M. Magnusson, A.-S. Smedman, 'Air flow behind wind turbines', *Journal of Wind Engineering and Industrial Aerodynamics*, vol. 80, pp. 169-189, 1999.

[25] J. F. Manwell, J. G. McGowan, A. L. Rogers, '*Wind Energy Explained: Theory, Design and Application*', 2009 John Wiley & Sons Ltd.

[26] D. Medici, P. H. Alfredsson, 'Measurements Behind Model Wind Turbines: Further Evidence of Wake Meandering', *Wind Energy*, vol. 11, pp. 211–217, 2008.

[27] T. Burton, N. Jenkins, D. Sharpe, E. Bossanyi, '*Wind Energy Handbook*', 2011, John Wiley & Sons, Ltd.

[28] K. Bose, '*Power Electronics and Motor Drives*', Elsevier, Oxford: 2003.